Energy transfers in magnetohydrodynamic shear turbulence

Energy transfers in magnetohydrodynamic shear turbulence

Journal of Physics: Conference Series **1522** (2020) 012005 doi:10.1088/1742-6596/1522/1/012005

Energy transfers in magnetohydrodynamic shear turbulence

Farrukh Nauman[1] and Anna Guseva[2]

[1]Department of Space, Earth and Environment, Chalmers University, SE-41296 Gothenburg, Sweden.

[2]School of Aeronautics, Universidad Poli'ecnica de Madrid, 28040 Madrid, Spain.

E-mail: farrukhnauman@gmail.com

Abstract. Astrophysical flows span a broad range of scales and thus require sub-grid modeling. We compute the energy fluxes in the Fourier and physical space for the turbulent magnetized shearing box simulations with a weak net vertical magnetic flux. The energy fluxes are dominated by the injection term from the mid-to-large scale range due to the Reynolds and Maxwell stresses in both cases while the small scales are dominated by dissipation. Since the nature of turbulent cascades requires a clear separation of scales, our work is unable to address these questions conclusively. But because our work is the first of its nature in trying to connect the Fourier and physical space energy flux behavior, we are able to make connections between the two profiles.

1. Introduction

Experiments and observations of fluids typically do not offer highly resolved data in either space or time. This is especially a problem for astrophysical fluids with extreme Reynolds number ($Re \geq 10^{12}$). For example, in the current state-of-the-art observations of disks around young stars the spatial resolution is $\sim 1AU = 10^{13}$ meters, as opposed to a dissipation scale of approximately 10^3 meters. Numerical modeling of magnetohydrodynamic (MHD) equations offers an opportunity to understand these high dimensional non-linear systems.

Keplerian flows are thought to be ubiquitous in accretion disks since the central gravitational source typically has a much higher mass than the disk. A stable background shear flow like this can be approximated by homogeneous shear flow. Hydrodynamic quasi-Keplerian velocity profiles, $V_\phi(r) \sim r^{-1/2}$, are hydrodynamically stable in Taylor-Couette experiments up to $Re = 10^5$ [15]. But the addition of a weak magnetic field makes Keplerian flows linearly unstable to magnetorotational instability (MRI: [4]). Shearing box simulations of magnetized Keplerian flows have been extensively studied both with [14] and without [19] a background magnetic flux. Both the lifetime of MHD turbulence and the non-linear characteristics of the developed turbulent state are sensitive to the ratio of viscosity and magnetic diffusivity (magnetic Prandtl number, Pm: [28, 19]).

Large Eddy Simulations (LES) offers a chance to model astrophysical fluids but they require understanding of multi-scale physics and chemistry. The cross-scale transfers of energy in fully developed turbulence can give insight into modeling sub-grid physics. Most sub-grid modeling relies on the presence of an 'inertial range' in the energy spectra that has universal behavior independent of the nature of injection and dissipation for a particular flow. Identifying the

regimes where those processes dominate is possible by studying different terms in the fluid equations in either spectral [9] or physical space [2, 8].

Kolmogorov phenomenological picture of turbulence requires that the nature of energy transfers is local-in-scale implying that direct exchanges of energy between the smallest and largest length scales of the flow do not occur. While this picture has been widely accepted in hydrodynamics, early work on spectral shell-to-shell transfers in magnetohydrodynamics suggested that a significant fraction of the energy transfer can be non-local [29, 1]. More recent work showed that the transfer in MHD is also local [3] if the spectra are binned logarithmically in spectral space instead of linearly. The argument relies on the basic idea that 'locality' should be defined as exchanges between powers of 2 (or some other base like 10), for example, instead of linearly spaced shells. Logarithmic binning is motivated by the power law behavior of the inertial range. Intuitively, for example in base 10, this means that the question of locality should be addressed in terms of transfers between distinct wavemode bands $K = 1 - 10$ and $K = 10 - 100$ instead of transfers between the same power of 10, say, $K = 1$ to $K = 9$. Using base 10 logarithmic binning, a significant energy transfer between $K = 1$ and $K = 99$ will still be considered 'local' as these are adjacent bands on the log scale.

The study of energy transfers can also address the direction of transfer: 'inverse' (small-to-large) as opposed to the 'direct' (large-to-small) transfers. In hydrodynamics, 2D turbulence leads to inverse energy cascade while 3D leads to a direct cascade. In MHD, even 3D turbulence can lead to an inverse cascade due to the conservation of magnetic helicity [7]. For MHD systems without a net helicity, energy cascades forward but still shows a pileup of energy on the largest scales. Understanding the co-existence of this dual cascade is an active topic of research and is currently limited by the dynamic range offered by state-of-the-art simulations.

Few works on non-linear energy transfers in Keplerian flows exist and all of them have used spectral space analysis using isotropy, an unrealistic but numerically convenient assumption. [12], [17] studied spectral transfers in homogeneous shear flows without and with a net magnetic flux in the computational box, respectively. The energy cascade was found to be direct but due to the lack of a clear inertial range, it remained unclear what kind of sub-grid models were appropriate. Some initial work on LES models for MHD shear flows [18] has shown some promise. In all of these works, anisotropic effects due to the magnetic field and shear were completely ignored to simplify the analysis. We adopt a similar approximation in our work here.

We study energy transfers in a homogeneous shear flow with a background magnetic flux that is unstable to the MRI. Our work is novel because we study both: (i) spectral and physical space transfers in MRI; (ii) $Pm < 1$ and $Pm \geq 1$ parameter regimes. The $Pm \leq 1$ limit is thought to be qualitatively distinct from the $Pm > 1$ due to different interaction of the magnetic and kinetic fields in the inertial and dissipative ranges of the spectra [23, 24]. We assume isotropy for numerical convenience and linearly spaced spherical shells in Fourier space. We leave the exploration of logarithmic binning in Fourier space and the study of anisotropy to future work.

We describe the numerical methods followed by a brief overview of the data in the next section. In the subsequent section, we discuss the physical and spectral energy transfers. We end with conclusions about the implications of our work.

2. Methods

No large publicly available databases on homogeneous shear MHD turbulence exist thus necessitating new Direct Numerical Simulations (DNS) to collect data for our analysis. We describe below the MHD equations, the code that we use, and parameters of the simulations used in this work.

2.1. Numerical method

We simulate incompressible MHD equations with a homogeneous shear flow using a pseudospectral solver SNOOPY [1] [16] (also known as the 'shearing box' in astrophysical literature). The MHD equations consist of the Navier-Stokes equation with the Lorenz force due to the magnetic field and the induction equation for the evolution of the magnetic fields. In dimensionless form they read:

$$\left(\frac{\partial}{\partial t} - Sx\frac{\partial}{\partial y}\right)\boldsymbol{V} = \boldsymbol{B}\cdot\nabla\boldsymbol{B} - \boldsymbol{V}\cdot\nabla\boldsymbol{V} + 2\Omega V_y\boldsymbol{e}_x - (2\Omega - S)V_x\boldsymbol{e}_y - \nabla\boldsymbol{\Pi} + \boldsymbol{B}_0\cdot\nabla\boldsymbol{B} + \nu\nabla^2\boldsymbol{V}, \tag{1}$$

$$\left(\frac{\partial}{\partial t} - Sx\frac{\partial}{\partial y}\right)\boldsymbol{B} = \boldsymbol{B}\cdot\nabla\boldsymbol{V} - \boldsymbol{V}\cdot\nabla\boldsymbol{B} - SB_x\boldsymbol{e}_y + \boldsymbol{B}_0\cdot\nabla\boldsymbol{V} + \eta\nabla^2\boldsymbol{B}, \tag{2}$$

where $\boldsymbol{V}$ and $\boldsymbol{B}$ are the velocity and magnetic field respectively. Both the velocity and magnetic fields are divergence free: $\nabla\cdot\boldsymbol{V} = 0 = \nabla\cdot\boldsymbol{B}$. The effective pressure, $\boldsymbol{\Pi}$, incorporates both hydrodynamic and magnetic pressure: $\boldsymbol{\Pi} = (p + B^2/2)$.

Units: The velocity field is scaled so that the shear parameter of the mean velocity $\boldsymbol{V}_{\rm sh} = -Sx\,\boldsymbol{e}_y$ is unity ($S = q\Omega = 1$). The factor $q = -d\ln\Omega/d\ln r = 3/2$ approximates Keplerian disks profile, and $\Omega = 2/3$ represents the angular frequency. The magnetic field is in the units of the Alfv́en speed, $v_A = B/\sqrt{\mu_0\rho} = B$ (magnetic permeability, $\mu_0 = 1 = \rho$). Time dimension is the 'shear time': $1/S$.

Initial conditions: We use a background magnetic field, $\boldsymbol{B} = B_0\boldsymbol{e}_z$ ($B_0 = 0.01$) that is conserved throughout the evolution of the MHD equations because of the periodic boundary conditions. Additionally, we apply random perturbations to the velocity with small amplitude (1% of the background shear) to low wavemodes.

Boundary conditions and resolution: The spatial resolution in the physical space is 256^3, which implies 256/3 de-aliased modes in Fourier space in each direction. The 'shear-periodic' boundary condition implies: $f(k_x, k_y, k_z, t) = f(k_x + Sk_yt, k_z, t)$.

Dimensionless parameters: The Reynolds, magnetic Reynolds and magnetic Prandtl numbers are defined as:

$$Re = SL_x^2/\nu, \quad Rm = SL_x^2/\eta, \quad Pm = Rm/Re. \tag{3}$$

The Reynolds and magnetic Reynolds number quantify the ratio between the advection and diffusion in velocity and magnetic fields respectively, and $Pm = \nu/\eta$ sets up the ratio of viscosity to magnetic dissipation.

2.2. Description of data

Forced isotropic MHD turbulence is hard to excite in the $Pm \ll 1$ regime with a Rm required to be above a threshold [23]. The same issue exists for homogeneous shear MHD flows [28, 19]. We study three different values of Pm to study whether the energy transfers are drastically different in these regimes. Table 1 provides a summary. Runs $Pm1$ and $Pm4$ are marginally under-resolved according to the criterion $k_{max}\lambda_{V,B} \gtrsim 1$. Here λ_V and λ_B are the Kolmogorov dissipation scales for velocity and magnetic fields respectively. A systematic comparison of energy transfers for a range of Pm has not been undertaken before as previous work focused on just one regime at a time: "ideal" non-resistive MHD ($\eta \to 0$) [11], $Pm < 1$ [17] or $Pm > 1$ [12].

MRI simulations have several time scales: 'shear' time ($t_S = 1/S$), most unstable MRI mode growth time ($t_{\rm MRI} \sim 1/\Omega$), 'viscous' ($t_\nu = L^2/\nu$) and 'resistive' times ($t_\eta = L^2/\eta$). More time scales can be defined using properties of the turbulent state. When choosing how long to evolve

[1] `http://ipag.osug.fr/~lesurg/snoopy.html`

Name	Re	Rm	$k_{max}\lambda_V$	$k_{max}\lambda_B$	$V^2/2S^2L^2$	$B^2/2S^2L^2$
Pm025	10000	2500	4.06	7.75	0.0029	0.0039
Pm1	10000	10000	0.82	0.69	0.29	2.47
Pm4	1000	4000	2.24	0.68	4.96	68.31

Table 1. Summary of the simulations used in this paper. We used a resolution of 256^3 and a box size of 1^3 for all of our simulations. The runs are named with the magnetic Prandtl number, $Pm = Rm/Re$. The energies grow with magnetic Prandtl number, which has been seen in previous simulations of MRI. Except $Pm025$ the simulations are not fully resolved.

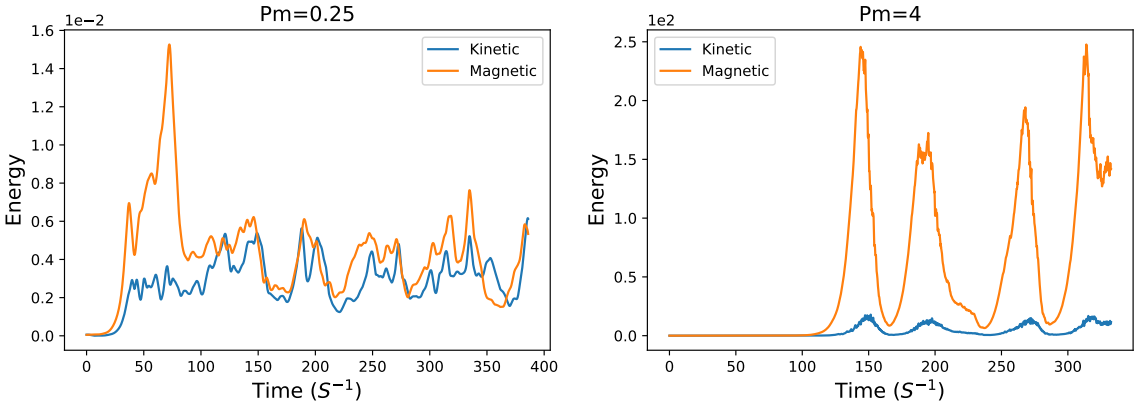

Figure 1. The time history of volume averaged energies. **Left**: For the $Pm = 0.25$ case, the energy amplitudes are roughly of the same magnitude and the corresponding evolution is quite similar as well except for the large initial spike early on in the evolution of the magnetic energy. **Right**: The magnetic energy is more than an order of magnitude larger than the kinetic energy for $Pm = 4$. The distinction between low and high Pm is one of the primary motivations for exploring energy transfers.

the simulations, one has to make sure that the important dynamics are captured such that the flow reaches a quasi-steady state in quadratic quantities like energy. On the other hand, longer evolution is computationally expensive. We made a compromise such that:

$$t_S, t_{\mathrm{MRI}} \ll t_f \ll t_\nu, t_\eta,$$

while also making sure that we capture at least two full cycle periods in the magnetic field (see figure 1: consecutive maxima imply one full cycle period in the magnetic field).

In figure 2, we show the time evolution of the Reynolds $\langle V_x V_y \rangle$ and Maxwell stresses $\langle -B_x B_y \rangle$. The Maxwell stresses always dominate the Reynolds stresses, a well known property of (linear) MRI with a net vertical field [21] that appears to hold in the non-linear regime as well. The "kinetic-to-magnetic" ratios of both energies and stresses are sensitive to the magnetic Prandtl number Pm as can be witnessed both in Figures 1, 2, and Table 1. Moreover, the fluctuations around the mean of time series happens on a slower time scale for low Pm as opposed to the high Pm case. In all the runs, Rm is considerably larger than unity that is consistent with the simulations of MRI in Taylor–Couette geometry indicate that Maxwell stresses dominate Reynolds stresses only if Rm is large enough [13].

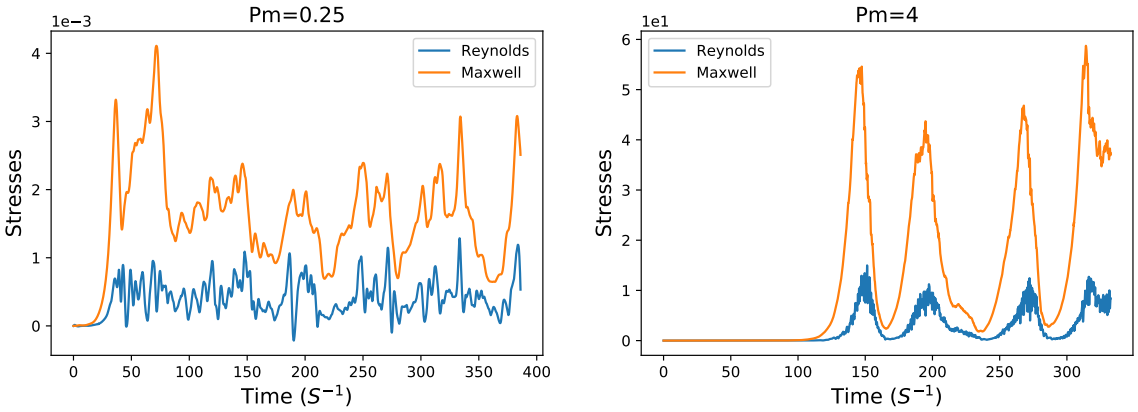

Figure 2. The volume averaged Reynolds ($\langle V_x V_y \rangle$) and Maxwell ($\langle -B_x B_y \rangle$) stresses both normalized with $S^2 L_x^2$. **Left**: The Maxwell stress remains larger than the Reynolds stress throughout the evolution unlike 1 where the magnetic energy even dips below the kinetic for a short time. **Right**: As the Pm has increased, the gap between the Reynolds and Maxwell stress increased as well. However, the difference is still less than an order of magnitude as opposed to the energies in fig 1.

3. Energy transfers

For our system, the steady state volume averaged energy equations reduce to:

$$S\langle V_x V_y \rangle - \langle B_j B_i \partial_j V_i \rangle = \nu \langle W^2 \rangle, \tag{4}$$

$$-S\langle B_x B_y \rangle + \langle B_j B_i \partial_j V_i \rangle = \eta \langle J^2 \rangle, \tag{5}$$

where $\boldsymbol{W} = \nabla \times \boldsymbol{V} =$ is the vorticity and $\boldsymbol{J} = \nabla \times \boldsymbol{B} =$ is the current density. The first term in both equations 4 and 5 are shear source terms that can be thought of as the 'injection' terms while the dissipation terms are on the right hand side of each equation. The second term on the left hand side represents the 'exchange' between velocity and magnetic fields. It is precisely this term that has caused confusion about whether the cascade in MHD turbulence is non-local [1, 3]. The exchange term only acts as a coupling term between the velocity and magnetic fields and does not contribute to the total volume averaged energy. Unlike the forced isotropic case [5], the exchange term $\langle B_j B_i \partial_j V_i \rangle$ is always negative since it is dominated by the Maxwell stress: $-B_x B_y > 0$ (see figure 2). The physical interpretation is that the energy injected by shear in the magnetic field is, on average, transformed into kinetic energy.

3.1. Fourier space transfers

We Fourier transform the fields using the definition:

$$\tilde{V}(\boldsymbol{k}) \equiv \int V(\boldsymbol{r}) \exp(-i\boldsymbol{k}\cdot\boldsymbol{r}) d^3\boldsymbol{r}, \qquad V(\boldsymbol{r}) = \frac{1}{(2\pi)^3} \int V(\boldsymbol{k}) \exp(i\boldsymbol{k}\cdot\boldsymbol{r}) d^3\boldsymbol{k}, \tag{6}$$

where $\boldsymbol{k}$ is the wavevector. The energy equations in Fourier space are:

$$\left(\partial_t - S\frac{k_x(t)k_y}{|k(t)|^2}\delta(|k(t)|-K)\right)\frac{|\tilde{V}|^2}{2} = \Re\left[\tilde{V}^*\cdot(\widetilde{B\cdot\nabla B}) - \tilde{V}^*\cdot(\widetilde{V\cdot\nabla V}) - \nu|\widetilde{W}|^2\right] + \Re\left[\tilde{V}^*\cdot(\widetilde{B_0 ik_z B}) + S\tilde{V}_y^*\tilde{V}_x\right], \tag{7}$$

$$\left(\partial_t - S\frac{k_x(t)k_y}{|k(t)|^2}\delta(|k(t)|-K)\right)\frac{|\tilde{B}|^2}{2} = \Re\left[\tilde{B}^*\cdot(\widetilde{B\cdot\nabla V}) - \tilde{B}^*\cdot(\widetilde{V\cdot\nabla B}) - \eta|\widetilde{J}|^2\right] + \Re\left[\tilde{B}^*\cdot(\widetilde{B_0 ik_z V}) - S\tilde{B}_y^*\tilde{B}_x\right]. \tag{8}$$

Here $K = \sqrt{k_x^2 + k_y^2 + k_z^2}$ and the asterisk represents complex conjugate. The second term on the left hand side is the shear advection term $-Sx\partial_y$ transformed to Fourier space. Its peculiar form originates from the time dependent nature of the x-component of the wavevector, $k_x(t) = k_{x0} + Stk_y$ (see the appendices in [17]).

Shell averaging: The flow is not isotropic because of magnetic fields and shear. We nonetheless consider isotropic shell averaging in this work due to simplified numerical analysis. The velocity and magnetic fields are averaged over linearly spaced (isotropic, for simplicity) spherical shells:

$$V_K(\boldsymbol{r}) = \sum_{K-\delta K/2<\boldsymbol{k}<K+\delta K/2} V(\boldsymbol{k})\exp(i\boldsymbol{k}\cdot\boldsymbol{r}), \tag{9}$$

where $\delta K = K_{n+1} - K_n$ for integer $n = 1 : K_{\max}$. With this definition, the power spectra of velocity and magnetic fields become $E^{\rm kin} = \langle V_K^2/2\rangle$ and $E^{\rm mag} = \langle B_K^2/2\rangle$ respectively. The angled brackets represent a spatial average. The non-linear transfer terms take the form: $\left\langle\left(\tilde{V}^*\cdot(\widetilde{V\cdot\nabla V})\right)_K\right\rangle$ and similarly for other transfer terms.

The delta function in the second term in equations 7 and 8 does not allow a direct calculation in each shell but averaging over shells of some size $(K_0 - \delta K/2, K_0 + \delta K/2)$ gets rid of the delta function. Because of periodic remapping, shear advection term is only significant 'locally' in a δK neighborhood. For convenience, we chose to only use snapshots where $t = T_s$ implying that $k_x(t) = k_x$. For further discussion on how to compute the shear advection term, see [17].

Earlier work on MRI energy transfers [10, 17, 18] found some evidence for law scaling for energy spectra with kinetic energy favoring a $K^{-3/2}$ scaling. Magnetic energy spectra power laws were not studied in these previous works as it did not show any clear power law range. For kinetic energy, we find similar results for $Pm = 1$ (left panel) figure 3 where the kinetic energy spectra is close to a $K^{-3/2}$ scaling for nearly one decade in modes whereas for $Pm = 4$ (right panel), no clear power law seems to hold for even one decade. The $K^{-3/2}$ power law is favored by Iroshnikov-Krachnan MHD turbulence model based on the assumption of 'strong magnetization'. The magnetic energy spectra in figure 4 shows hints of a power law but just like the kinetic energy spectra in figure 3, it does not have enough range in scales.

Spectral transfers plotted in figure 5 cannot tell us about the locality of transfer but can tell us about the *direction* of cascade. The sum of all the transfer terms is positive in all cases indicating a net transfer of energy forwards. The most noticeable feature of these plots is that the injection term $(V_xV_y - B_xB_y)$ dominates all other terms in the Fourier transfers for the first few modes whereas for larger modes, the dissipation term starts to become significant. It is, therefore, unclear that the decade $KL/2\pi = 2 : 20$ of $K^{-3/2}$ seen in the left panel of figure 3 can be termed an 'inertial' range. These plots are consistent with existing work [11, 17] that similarly found that the injection term is dominant across a range of modes thus making the identification of an inertial range quite difficult despite hints of a power law in the kinetic energy spectra.

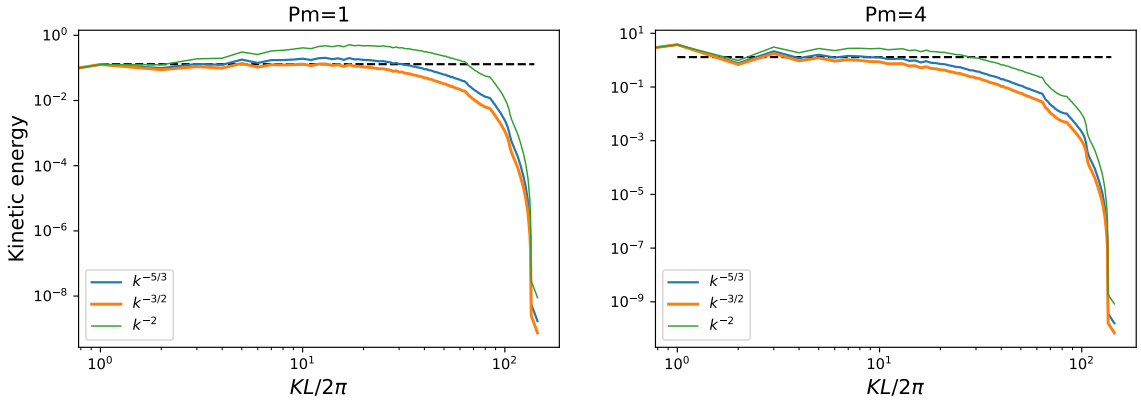

Figure 3. Pre-multiplied shell averaged spectrum of the kinetic energies. **Left**: The kinetic energy for $Pm = 1$ seems to follow a $K^{-3/2}$ (orange) power law for roughly a decade ($KL/2\pi = 2 : 20$). **Right**: For $Pm = 4$, the spectrum is closer to $K^{-5/3}$ (blue) but does not last for even one decade. The dashed straight line acts as a guide.

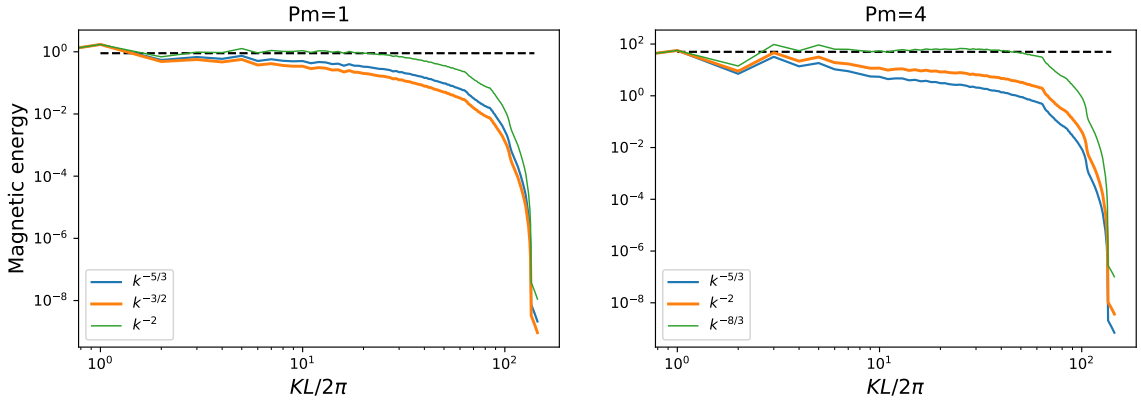

Figure 4. Pre-multiplied shell averaged spectrum of the magnetic energies. **Left**: The power law for $Pm = 1$ seems to behave as K^{-2} (green). **Right**: The $Pm = 4$ spectrum is steeper as the spectrum is closer to $K^{-8/3}$ (green).

The non-linear transfer terms remain sub-dominant for the entire range of modes. The shear advection term (red) appears to be significant for an intermediate range for the $Pm = 1$ case, which is similar to the behavior of the $Pm = 4$ run reported in [12] where the shear advection term dominated all other terms.

3.2. Physical space transfers

For studying energy transfers in physical space, we use the Gaussian filter:

$$\overline{\boldsymbol{V}}_\ell(\boldsymbol{x}) = \int d^3r G(\boldsymbol{r}) \boldsymbol{V}(\boldsymbol{x}+\boldsymbol{r}) \tag{10}$$

where the $\overline{\boldsymbol{V}}_\ell$ is the physical space filtered velocity and the Gaussian filter is defined as

$$G(x) = \frac{1}{(2\pi\ell^2)^{3/2}} \exp(-r^2/2\ell^2) \tag{11}$$

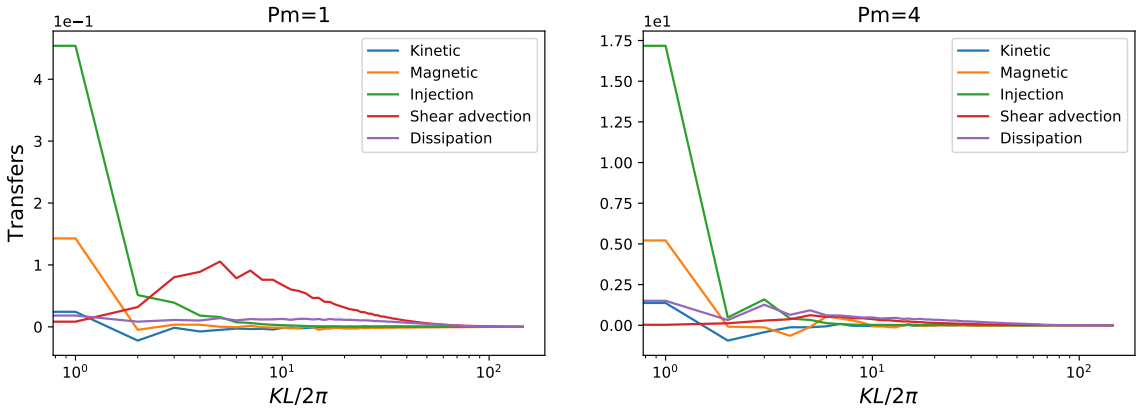

Figure 5. The nonlinear transfer terms in the induction equation. The kinetic non-linear term refers to $Re[\tilde{V}^* \cdot (\widetilde{B \cdot \nabla B}) - \tilde{V}^* \cdot (\widetilde{V \cdot \nabla V})]$ while the magnetic term is $Re[\tilde{B}^* \cdot (\widetilde{B \cdot \nabla V}) - \tilde{B}^* \cdot (\widetilde{V \cdot \nabla B})]$. The injection term is: $S(\tilde{V}_y^* \tilde{V}_x - \tilde{B}_y^* \tilde{B}_x)$. **Left**: For $Pm = 1$, the injection term (green) dominates for the first few modes and then the shear advection term (red) takes over. **Right**: Similar spectral profiles of all terms except that in this case the shear advection term does not become significant.

where ℓ is the filter length and $r^2 = x^2+y^2+z^2$. Since we work in a periodic box, the convolution in equation 10 translates into a multiplication in Fourier space: $\overline{\boldsymbol{V}}_\ell(\boldsymbol{k}) = G(K,\ell)\,\boldsymbol{V}(\boldsymbol{k}) = \exp(-K^2\ell^2/2)\,\boldsymbol{V}(\boldsymbol{k})$. Here $K = \sqrt{k_x^2 + k_y^2 + k_z^2}$ has the same definition as it did in equations 7 and 8. In Fourier space, the 'fluctuating' field is simply $(1 - G(K,\ell))\,\boldsymbol{V}(\boldsymbol{k})$. We use an isotropic filter for simplicity but since we are studying a magnetized shear flow, anisotropies are likely to play a strong role. We leave this for future work.

The shear advection term does not commute with the Gaussian filter:

$$\overline{(x\partial_y V)}_\ell = x\partial_y \overline{V}_\ell + \ell^2 \partial_x \partial_y \overline{V}_\ell. \tag{12}$$

The other terms commute and so the equation has the form:

$$(\partial_t - Sx\partial_y)\frac{\overline{V}_\ell^2}{2} - S\ell^2\partial_x\partial_y\frac{\overline{V}_\ell^2}{2} + \nabla\cdot(\ldots) = -\Pi_\ell^V - \overline{B}_{\ell,i}\overline{B}_{\ell,j}\partial_j\overline{V}_{\ell,i} - \nu\overline{W}_\ell^2 - \overline{B}_{\ell,i}B_0\partial_z\overline{V}_{\ell,i} + S\overline{V}_{\ell,x}\overline{V}_{\ell,y}, \tag{13}$$

$$(\partial_t - Sx\partial_y)\frac{\overline{B}_\ell^2}{2} - S\ell^2\partial_x\partial_y\frac{\overline{B}_\ell^2}{2} + \nabla\cdot(\ldots) = -\Pi_\ell^B + \overline{B}_{\ell,i}\overline{B}_{\ell,j}\partial_j\overline{V}_{\ell,i} - \eta\overline{J}_\ell^2 + \overline{B}_{\ell,i}B_0\partial_z\overline{V}_{\ell,i} - S\overline{B}_{\ell,x}\overline{B}_{\ell,y}. \tag{14}$$

Here the flux terms represented by ellipsis are ignored since we volume average over a periodic domain and so these flux terms average to zero. The nonlinear transfer terms are [2]:

$$\Pi_\ell^V = -\partial_j\overline{V}_{\ell,i}\left(\overline{(V_iV_j)}_\ell - \overline{V}_{\ell,i}\overline{V}_{\ell,j} - (\overline{(B_iB_j)}_\ell - \overline{B}_{\ell,i}\overline{B}_{\ell,j})\right),$$
$$\Pi_\ell^B = -\partial_j\overline{B}_{\ell,i}\left(\overline{(V_jB_i)}_\ell - \overline{V}_{\ell,j}\overline{B}_{\ell,i} - (\overline{(V_iB_j)}_\ell - \overline{V}_{\ell,i}\overline{B}_{\ell,j})\right).$$

These represent the energy transferred from the large scales $l > \ell$ to the small scales $l < \ell$ and depending on the properties of these terms, an appropriate sub-grid model can be chosen to represent scale invariant behavior of the system in the inertial range.

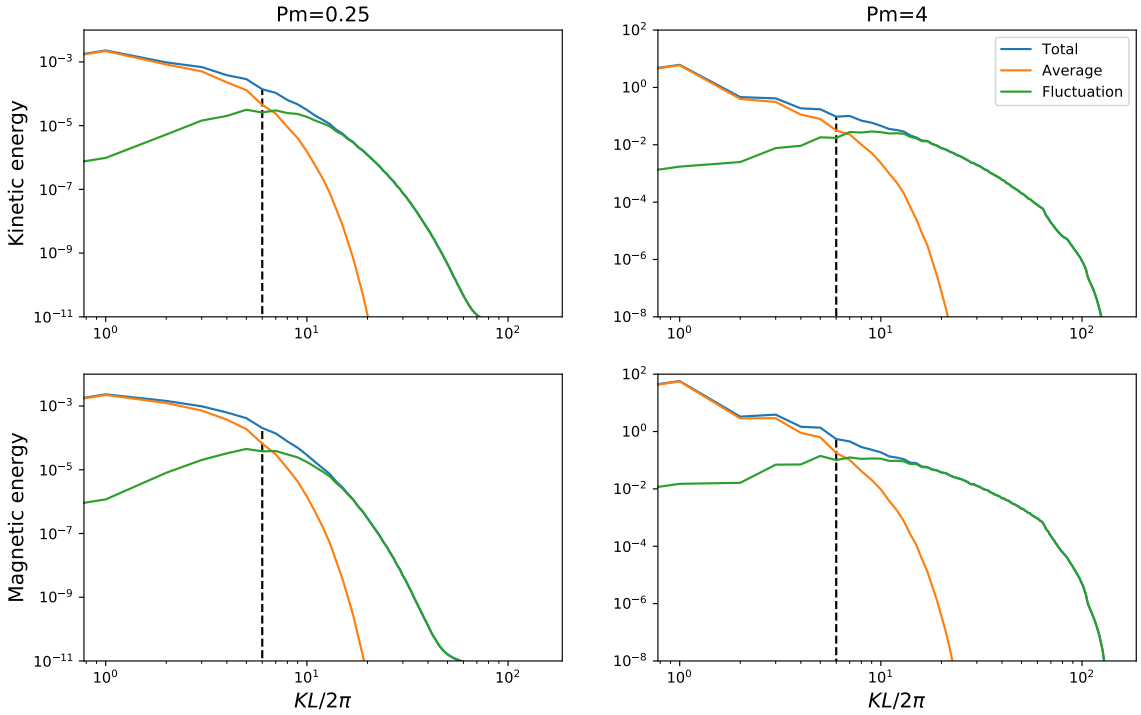

Figure 6. Shell averaged spectrum of the energies with Gaussian filter with length $\ell = 0.0265$ ($K\ell/2\pi = 6$: vertical dashed line). **Left**: For $Pm = 0.25$, the peak at small modes is not as pronounced but still the Gaussian filtered field contains most of the energy. The magnetic energy (bottom) dissipates earlier than the kinetic energy as is expected for $Pm < 1$. The integral scales for both kinetic and magnetic energy are separated by a few modes ($2\pi/L_{int} \sim 1.9, 5.5$ for the smoothed and fluctuating fields respectively). **Right**: For $Pm = 4$, the spectra extend all the way to K_{max} but have a stronger dominance of the first few modes. The integral scales for both kinetic and magnetic energy are separated by a few modes ($2\pi/L_{int} \sim 1.6, 7.0$ for the smoothed and fluctuating fields respectively).

In figure 6, we show the kinetic and magnetic energies for two runs $Pm = 0.25$ (left column) and $Pm = 4$ (right column). The $Pm = 0.25$ energies are truncated at lower wavemodes because they are highly resolved (see table: 1). The Gaussian filtered fields for the the kinetic and magnetic energy have similar behavior: they both account for most of the energy in the system because the energy spectra are dominated by the first few modes. The integral scales for kinetic and magnetic energies in each of the runs are separated by a few modes indicating the difference in dominant scales for velocity and magnetic fields with the caveat that we use an isotropic filter.

We computed a spectrum-like plot in figure 7 for Gaussian filters using a three step process:

(i) Apply the Gaussian filter for a given length ℓ for each term in equations 13, 14.

(ii) Looped over $\ell = 1, 4, 8, ..., 148$ in steps of 4.

(iii) Volume average over the whole domain and time average over 20 snapshots.

The amplitude of large-scale (filtered) fields increase as the filtering length approaches dissipation scale. The interpretation of the Gaussian filtered terms is different from the Fourier spectra: the Gaussian filtered quantities can be thought of as a 'cumulative' spectrum where all the energy up to a certain length scale is included for a quantity at length, 'ℓ'. This causes

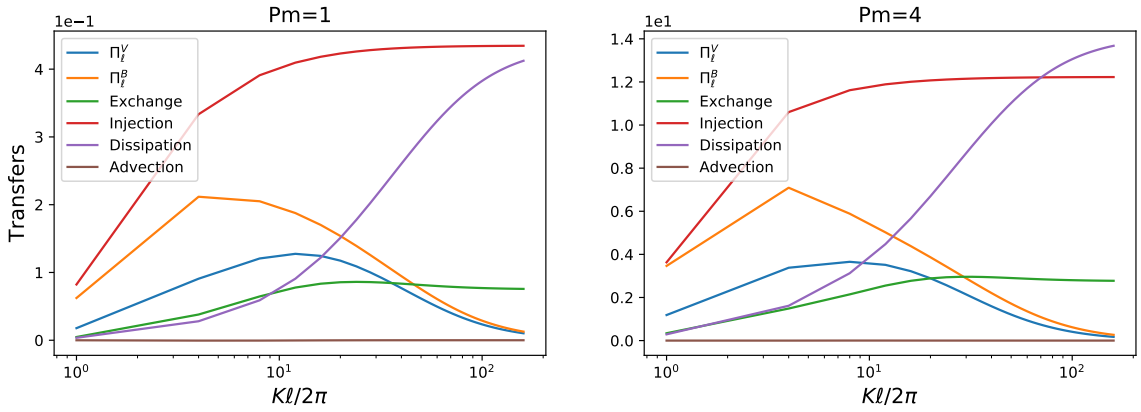

Figure 7. The spatial and temporal mean of linear and nonlinear terms that have been Gaussian filtered at each wavenumber, $K_{filt} = 2\pi/\ell$ in Fourier space. The term labels represent different terms in equations 13, 14. The exchange term is plotted as $-\overline{B}_{\ell,i}\overline{B}_{\ell,j}\partial_j\overline{V}_{\ell,i}$, which is always positive. For both $Pm = 1$ (**left**) and $Pm = 4$ (**right**), the non-linear transfer terms compete with each other at large filter lengths while being overshadowed by the much stronger injection term.

the large-scale terms such as the exchange and injection terms to increase with $K\ell/2\pi$ (fig. 7)). The (shear) injection term (red) only acts on scales: $\ell \gtrsim 2\pi/10$ and is thus consistent with the physical intuition that shear is a large scale effect. Given the limited resolution of these simulations, the dissipation term already starts to dominate beyond $\ell \gtrsim 2\pi/10$ implying that an inertial range simply does not exist. The shear advection term that dominated the $Pm = 1$ Fourier transfer plots in figure 5 is zero for Gaussian filters. This is because we computed a spatial volume average, which due to periodic boundary conditions reduces the $\langle\partial_x()\rangle = 0$.

Recently [5] found that the cascade of the kinetic and magnetic energies are coupled in the intermediate to large scales (within the inertial range) through the $-\overline{B}_{\ell,i}\overline{B}_{\ell,j}\partial_j\overline{V}_{\ell,i}$ term while they are decoupled from the small to intermediate scales (within the inertial range) in isotropic forced MHD simulations. We find that while $-\overline{B}_{\ell,i}\overline{B}_{\ell,j}\partial_j\overline{V}_{\ell,i}$ is smaller than the non-linear kinetic (Π^V) and magnetic transfers (Π^B) up to $K\ell/2\pi \sim 40$, the exchange term only starts to become significant compared to the non-linear terms in the dissipation regime. The difference between our results and the forced isotropic turbulence in [5] could come from: (i) the non-local nature of the injection term as opposed to forced isotropic turbulence where the injection term is restricted to a small band; (ii) lack of resolution since [5] use up to 2048^3 simulations whereas we restrict ourselves to 256^3. Indeed a clear inertial range is hard to achieve in even in low resolution homogeneous isotropic turbulence simulations.

3.3. Comparing Fourier and Gaussian spectra

Gaussian filtered quantities are cumulative: $\overline{V}_\ell$ contains contributions from *all* scales $l < \ell$. In contrast, Fourier transformed quantities represent the values of the field at each wavenumber ($K \sim \ell^{-1}$). Gaussian filtered quantities can be related to Fourier power spectra using $\ell - shells$: $E^{Fourier}(K_\ell) \sim E^{Gaussian}(K_{\ell_2}) - E^{Gaussian}(K_{\ell_1})/\delta\ell$ [26]. Similar shell-to-shell computations can be done for transfer terms in physical space (or alternatively cumulative spectra in Fourier space) but this is beyond the scope of the current work.

4. Conclusions

We explored $Pm = 0.25, 1.0, 4.0$ in this work, which at face value might appear to be a small range but the three runs show qualitatively different behavior. Indeed the $Pm = 0.25$ run has a spectrum that truncates earlier than other runs and is highly resolved with the same resolution where the other two runs are marginally resolved. We analyzed the energy transfers in both Fourier space and physical space (using Gaussian filters) and found that the energy injection term dominates in both cases. Our main conclusions are:

- A clear inertial range does not exist because: (i) injection term due to Reynolds and Maxwell stresses is effective at mid-to-large scales; and because of small Re, Rm and resolution, (ii) the dissipation dominates the small-to-mid scales.
- In contrast to hydrodynamically forced isotropic turbulence, magnetic energy feeds kinetic energy through the exchange term.

Our work highlights challenges for constructing meaningful sub-grid models for MHD fluids with a homogeneous shear. Overall, our results suggest that turbulent MHD homogeneous shear flows are significantly different from homogeneous isotropic turbulence where a clear separation between the injection and dissipation scales exist. The lack of a clear inertial range could be the result of modest resolution of 256^3 or it could be a property of magnetized homogeneous shear flows. Future work with high resolution simulations might offer insight into this question.

We considered only isotropic shell averaging in Fourier space and isotropic Gaussian filters in physical space. Homogeneous magnetized shear flows are known to be strongly anisotropic, which highlights a major limitation of our work. Furthermore, we only considered isotropic domains further restricting the development of strong anisotropic structures. We only considered linearly spaced bins in Fourier space instead of logarithmic binning. The comparison between Fourier and physical space further suffers from the differences in the nature of the two approaches: Fourier space analysis is not cumulative while Gaussian physical space analysis is. We hope to address these limitations in future work.

Acknowledgements

This work was supported in part by the Coturb project of the European Research Council, and performed during the 4th. Madrid summer workshop on turbulence. We are grateful to Alberto Vela–Martín for his careful review of an early version of this manuscript.

References

[1] Alexakis A., Mininni P. D., and Pouquet A., 2005 Shell-to-shell energy transfer in magnetohydrodynamics. I. Steady state turbulence. *Phys. Rev.* E **72**:046301
[2] Aluie H. 2017 Coarse-grained incompressible magnetohydrodynamics: analyzing the turbulent cascades. *New. J. Phys.* **19**:025008
[3] Aluie H. and Eyink G. L. 2010 Scale locality of magnetohydrodynamic turbulence. *Phys. Rev. Lett.* **104**, 081101
[4] Balbus S. A. and Hawley J. F. 1998 Instability, turbulence, and enhanced transport in accretion disks. *Rev. Mod. Phys.* **70**:1–53.
[5] Bian, X. and Aluie, H. 2019 Decoupled cascades of kinetic and magnetic energy in magnetohydrodynamic turbulence. *Phys. Rev. Lett.* **122**:135101
[6] Bodo G., Mignone A., Cattaneo F., Rossi P. and Ferrari A. 2008 Aspect ratio dependence in magnetorotational instability shearing box simulations. *A. & A.* **487**:1–5.
[7] Brandenburg A. 2001 The inverse cascade and nonlinear alpha-effect in simulations of isotropic helical hydromagnetic turbulence. *ApJ* **550**:824–840.
[8] Camporeale E., Sorriso-Valvo L., Califano F. and Retinò A. 2018 Coherent structures and spectral energy transfer in turbulent plasma: a space-filter approach. *Phys. Rev. Lett.* **120**:125101
[9] Davidson P. A. 2004 *Turbulence: an introduction for scientists and engineers.* (Oxford Univ. Press)
[10] Fromang S. 2010 MHD simulations of the magnetorotational instability in a shearing box with zero net flux: the case Pm = 4. *A. & A.* **514**:L5

[11] Fromang S. and Papaloizou J. 2007 MHD simulations of the magnetorotational instability in a shearing box with zero net flux. I: The issue of convergence. *A. & A.* **476**:1113-1122.
[12] Fromang S., Papaloizou J., Lesur G. and Heinemann T. 2007 MHD simulations of the magnetorotational instability in a shearing box with zero net flux. II: The effect of transport coefficients. *A. & A.* **476**:1123–1132.
[13] Guseva, A., Willis, A. P., Hollerbach, R., Avila, M. 2017 Transport properties of the azimuthal magnetorotational instability. *ApJ* **849**:92
[14] Hawley J. F., Gammie C. F., Balbus S. A., 1995 Local three-dimensional magnetohydrodynamic simulations of accretion disks. *ApJ* **440**:742–763.
[15] Ji H., Burin M., Schartman E., and Goodman J. 2006 Hydrodynamic turbulence cannot transport angular momentum effectively in astrophysical disks. *Nature* **444**: 343-346.
[16] Lesur G., and Longaretti P.-Y. 2007 Impact of dimensionless numbers on the efficiency of magnetorotational instability induced turbulent transport. *MNRAS* **378** 1471-1480.
[17] Lesur G., and Longaretti P.-Y. 2011 Non-linear energy transfers in accretion discs MRI turbulence. I: Net vertical field case. *A. & A.* **528**:A17
[18] Meheut H., Fromang S., Lesur G., Joos M. and Longaretti P.-Y. 2015 Angular momentum transport and large eddy simulations in magnetorotational turbulence: the small Pm limit. *A. & A.* **579**:A117
[19] Nauman F. and Pessah M. E. 2016 Sustained turbulence in differentially rotating magnetized fluids at a low magnetic Prandtl number. *ApJ* **833**:187
[20] Nauman F. and Pessah M. E. 2018 Transport properties of Keplerian flows in extended local domains with no imposed field. *MNRAS* **480**:204–209.
[21] Pessah M. E., Chan C.-K., and Psaltis D. 2008 The fundamental difference between shear alpha viscosity and turbulent magnetorotational stresses. *MNRAS* **383**:683-690.
[22] Riols A., Rincon F., Cossu C., Lesur G., Ogilvie G. I., and Longaretti P.-Y. 2015 Dissipative effects on the sustainment of a magnetorotational dynamo in Keplerian shear flow. *A. & A.* **575**:A14
[23] Schekochihin A. A., Haugen N. E. L., Brandenburg A., Cowley S. C., Maron J. L. and McWilliams J. C. 2005 The onset of a small-scale turbulent dynamo at low magnetic Prandtl numbers. *ApJL* **625**:L115-L118.
[24] Schekochihin A. A., Iskakov A. B., Cowley S. C., McWilliams J. C., Proctor M. R. E. and Yousef T. A. 2007 Fluctuation dynamo and turbulent induction at low magnetic Prandtl numbers. *New. J. Phys.* **9**:300
[25] Sekimoto A., Dong S. and Jiménez J. 2016 Direct numerical simulation of statistically stationary and homogeneous shear turbulence and its relation to other shear flows . *Phys. Fluids* **28**:035101
[26] Sadek, M., Aluie, H. 2018 Extracting the spectrum of a flow by spatial filtering. *Phys. Rev. Fluids* **3**:124610
[27] Shakura N. and Postnov K. 2015 On properties of Velikhov–Chandrasekhar MRI in ideal and non-ideal plasma. *MNRAS* **448**:3697-3706.
[28] Shi J.-M., Stone J. M. and Huang C. X. 2016 Saturation of the magnetorotational instability in the unstratified shearing box with zero net flux: convergence in taller boxes. *MNRAS* **456**:2273-2289.
[29] Verma M. K. 2004 Statistical theory of magnetohydrodynamic turbulence: recent results. *Phys. Rep.* **401** 229-380.